Current-Induced Torques with Dresselhaus Symmetry Due to Resistance Anisotropy

Gregory M. Stiehl,[†] David MacNeill,[†] Nikhil Sivadas,[‡] Ismail El Baggari,[‡] Marcos H. D. Guimarães,[†,¶] Neal D. Reynolds,[†] Lena F. Kourkoutis,[‡,¶] Craig Fennie,[‡] Robert A. Buhrman,[‡] and Daniel C. Ralph[*,†,¶]

†*Department of Physics, Cornell University, Ithaca, NY 14853, USA*

‡*Department of Applied and Engineering Physics, Cornell University, Ithaca, NY 14853, USA*

¶*Kavli Institute at Cornell, Cornell University, Ithaca, NY 14853, USA*

E-mail: dcr14@cornell.edu

Abstract

We report measurements of current-induced torques in bilayers of Permalloy (Py) with $TaTe_2$, a transition-metal dichalcogenide material possessing low crystal symmetry, and observe a torque component with Dresselhaus symmetry. We suggest that the dominant mechanism for this Dresselhaus component is not a spin-orbit torque, but rather the Oersted field arising from a component of current that flows perpendicular to the applied voltage due to resistance anisotropy within the $TaTe_2$. This identification broadens the class of mechanisms that must be considered when analyzing the origins of unusual current-induced torques generated by materials with low crystal symmetry within magnetic heterostructures.

Current-induced spin-orbit torques are a promising method for efficiently manipulating magnetic devices.[1] Understanding the mechanisms by which the directions of these torques can be manipulated, for example by using crystal symmetries, is important for optimizing them for applications. To date, all observations of spin-orbit torques from centrosymmetric materials – generated through either spin Hall,[2,3] Rashba-Edelstein,[4,5] topological spin-momentum locking,[6,7] or other spin-orbit effects[8,9] – can be described as corresponding to a Rashba-like symmetry (Fig. 1a). That is, the generated field or spin is perpendicular to the applied current and lies within the sample plane. Torques corresponding to a more general spin symmetry have been observed only in non-centrosymmetric systems, such as torques resulting from the out-of-plane spins in WTe_2,[10,11] or torques corresponding to a Dresselhaus-like spin polarization (Fig. 1b) observed in GaMnAs,[12,13] GaAs/Fe bilayers[14,15] and NiMnSb.[16] Here, we analyze current-induced torques in bilayers of Permalloy ($Py = Ni_{81}Fe_{19}$) with the low-symmetry material $TaTe_2$, a centrosymmetric transition-metal dichalcogenide (TMD). To our surprise, the heterostructures exhibit a component of field-like torque for which the dependence on the angle of applied current relative to the crystalline axes reflects a Dresselhaus symmetry, despite the fact that $TaTe_2$ is inversion symmetric. We suggest that in $TaTe_2$ this torque does not originate from a spin-orbit mechanism. Instead, it likely arises from resistance anisotropy within the plane of the $TaTe_2$ layers, which can cause current flow non-collinear with the applied electric field, leading to an Oersted field that mimics a Dresselhaus symmetry. This effect will modify the form of current-induced torques produced by any low-symmetry source material, and might be used beneficially to engineer the direction of the Oersted torque to assist switching in memory devices.[17]

$TaTe_2$ at room temperature has a monoclinic (1T') crystal structure with a centrosymmetric space group C2/m (# 12).[18,19] When integrated into a heterostructure with Py only a single structural symmetry remains: a mirror plane perpendicular to the TMD layers. In $TaTe_2$, this mirror is within the a-c plane, (Fig. 1c). The low-symmetry crystal structures of $TaTe_2$ is clearly visible in the cross-sectional high-angle annular dark-field scanning

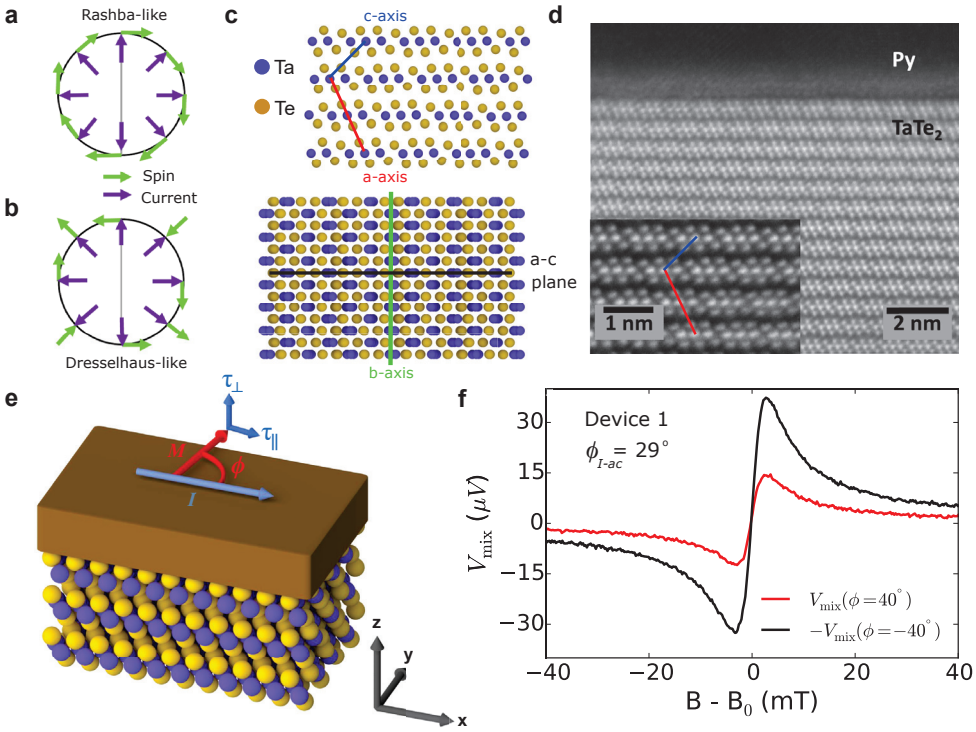

Figure 1: (a) Rashba-like and (b) Dresselhaus-like net spin (or field) polarizations, where the spin (green arrow) is generated in response to an applied current (purple arrow). The grey line represents a mirror plane. (c) $TaTe_2$ crystal structure looking down the b-axis (top) and the exfoliation plane (bottom). The yellow spheres represent Te atoms and the purple spheres represent Ta atoms. (d) A cross-sectional HAADF-STEM image of a $TaTe_2$/Permalloy device showing high crystallinity except for a region at the $TaTe_2$/Py interface approximately one $TaTe_2$ layer thick. In all other layers, the trimerization associated with the low-symmetry room-temperature $TaTe_2$ crystal structure is clearly visible. (Inset) a HAADF-STEM image of the same device with higher magnification, clearly showing the low-symmetry structure. (e) Schematic of the bilayer $TaTe_2$/Permalloy sample geometry. The x-axis is defined to be parallel to the applied electric field and the z-axis is perpendicular to the sample plane. (f) ST-FMR resonances for a $TaTe_2$ (19.7 nm) / Py (6 nm) device (Device 1) with the magnetization oriented at 40° and -40° degrees with respect to the current direction. The applied magnetic field, B, is normalized by the resonance field, B_0, to account for a small shift in the resonance due to an in-plane uniaxial anisotropy in the Permalloy. The applied microwave power is 2 dBm at a frequency of 9 GHz.

transmission electron microscopy (HAADF-STEM) image of one of our devices (Fig. 1d).

To fabricate our samples we exfoliate $TaTe_2$ from bulk crystals (supplied by HQ graphene) onto high resistivity silicon / silicon oxide wafers using the scotch tape method, where the final step of exfoliation is carried out in the load lock of our sputtering system under high vacuum ($< 10^{-6}$ torr). Without breaking vacuum, we then deposit 6 nm of the ferro-

magnet permalloy (Py = $Ni_{81}Fe_{19}$) by grazing angle sputtering to minimize damage to the $TaTe_2$ surface (Fig. 1d) in an Ar pressure of 4 mtorr. We use a deposition rate below 0.2 angstroms/second, with the substrate rotating at greater than 10 revolutions per minute. To prevent oxidation of the ferromagnet we cap the bilayers with 2 nm of Al, which is oxidized upon exposure to atmosphere. Flakes for further processing are selected *ex situ* using optical and atomic force microscopy. All devices are positioned so that the active region is atomically flat, with an RMS surface roughness below 300 pm and no monolayer steps. The devices are patterned using e-beam lithography into either a microwave-frequency-compatible ground-signal-ground geometry for resonant measurements, or Hall bars for low-frequency (kHz) 2nd-harmonic Hall measurements, with pattern transfer by Ar ion milling with SiO_2 used as an etch mask. The etched devices are protected by subsequent sputter coating of SiO_2. Electrical contacts, Ti (5 nm) / Pt (75 nm), are defined through a lift-off process.

We characterize the angle ϕ_{I-ac} between the direction of the applied current and the mirror plane of the TMD in the finished devices by measurements of a magnetic easy axis in the Py induced by interaction with the TMD,[10,11,20] in combination with polarized Raman spectroscopy and HAADF-STEM imaging (see Supporting Information). The Py equilibrium magnetization direction, $\hat{m}$, lies within the sample plane. As depicted in Fig. 1e, when a current is applied to a TMD/Py bilayer a current-induced torque acts on the magnetic moment. To measure the current-induced torques in our samples, we use two complementary measurement methods, a harmonic Hall technique,[11,21,22] and spin-torque ferromagnetic resonance (ST-FMR),[2,6,10] with all measurements made at room temperature. Both types of measurements gave consistent results. The harmonic Hall measurements are detailed in the Supporting Information.

In the ST-FMR measurements, an in-plane RF current (7-12 GHz) is applied to the sample which generates torques on the ferromagnet in phase with the current (Fig. 1e). An in-plane magnetic field is applied at an angle of ϕ relative to the applied current, and the magnitude of this field is swept through the ferromagnetic resonance condition. We measure

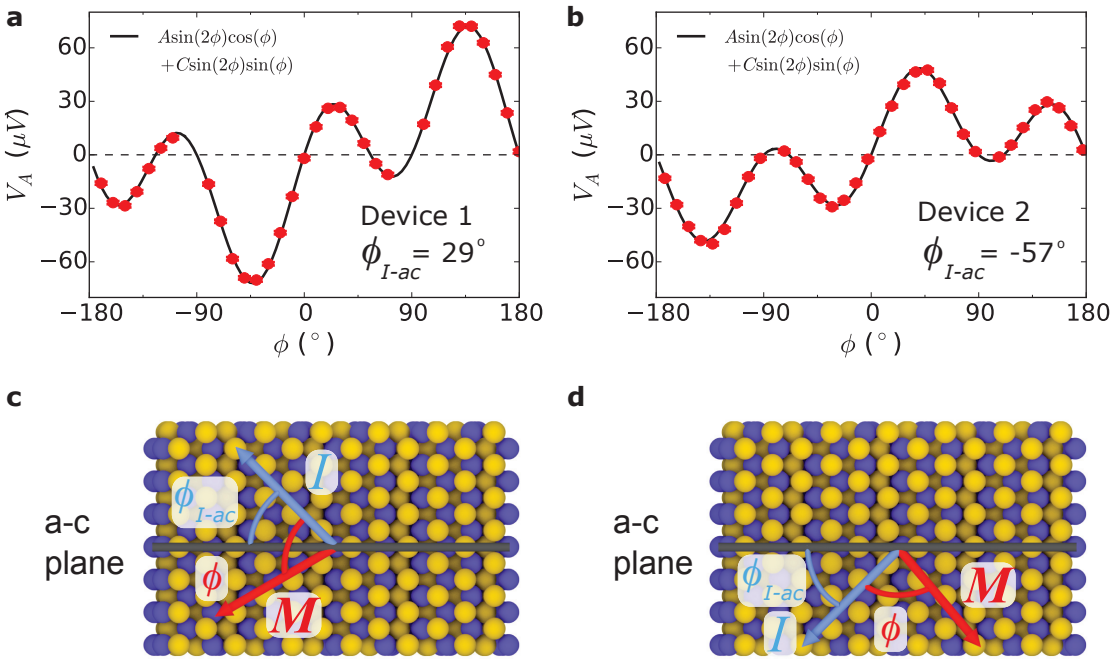

Figure 2: (a) and (b) Antisymmetric component of the ST-FMR resonance as a function of applied in-plane magnetic field angle for $TaTe_2$/Py Devices 1 and 2 respectively. The applied microwave power is 2 dBm at a frequency of 9 GHz. Device 1 is $TaTe_2$ (19.7 nm) / Py (6 nm) and Device 2 is $TaTe_2$ (8.8 nm) / Py (6 nm). The value of ϕ_{I-ac}, the angle between the current and $TaTe_2$ a-c mirror plane, is 29° in panel (a) and -57° in panel (b). (c) and (d) depict a positive and negative ϕ_{I-ac} angle, respectively, corresponding to Devices 1 and 2, and ϕ is depicted as positive for both (c) and (d).

a DC voltage arising from mixing between the RF current and resistance oscillations resulting from magnetization precession together with the anisotropic magnetoresistance (AMR) of the Py (Fig. 1f). This mixing voltage, V_{mix}, can be fitted as a function of magnetic field as a sum of symmetric and antisymmetric Lorentzians, where the amplitudes of these resonances (V_S and V_{A}) allow independent measurements of the in-plane ($\vec{\tau}_{\parallel}$) and out-of-plane ($\vec{\tau}_{\perp}$) spin-orbit torques respectively:[2,10]

$$V_{\text{S}} = -\frac{I_{\text{RF}}}{2}\left(\frac{dR}{d\phi}\right)\frac{1}{\alpha_{\text{G}}\gamma\left(2B_0+\mu_0 M_{\text{eff}}\right)}\tau_{\parallel}, \tag{1}$$

$$V_{\text{A}} = -\frac{I_{\text{RF}}}{2}\left(\frac{dR}{d\phi}\right)\frac{\sqrt{1+\mu_0 M_{\text{eff}}/B_0}}{\alpha_{\text{G}}\gamma\left(2B_0+\mu_0 M_{\text{eff}}\right)}\tau_{\perp}. \tag{2}$$

Here R is the device resistance, $dR/d\phi$ is due to the AMR in the Py, $\mu_0 M_{eff}$ is the out-of-plane demagnetization field, B_0 is the resonance field, I_{RF} is the microwave current in the bilayer, α_G is the Gilbert damping coefficient, and the equilibrium magnetization is saturated along the applied field direction.

The magnitude of torques with a conventional Rashba-like symmetry, $\vec{\tau}_{\parallel} \propto \hat{m} \times (\hat{m} \times \hat{y})$ and $\vec{\tau}_{\perp} \propto \hat{m} \times \hat{y}$ for current in the $\hat{x}$ direction, are proportional to $\cos(\phi)$. Therefore, in the presence of only Rashba-like torques the magnitude of V_{mix} is unchanged upon the operation $\phi \rightarrow -\phi$ but the sign is reversed (as $dR/d\phi \propto \sin(2\phi)$ in Eqs. 1 and 2). Figure 1f shows resonance curves in V_{mix} as a function of applied in-plane field magnitude for $\phi = 40°$ (red) and $\phi = -40°$ (black, inverted), for one of our $TaTe_2$/Py bilayer devices (Device 1). The difference between the two V_{mix} measurements shows a lack of $\phi \rightarrow -\phi$ symmetry in the observed torques and suggests the presence of a torque which does not arise entirely from a Rashba-like spin polarization. For all of the $TaTe_2$/Py devices, the antisymmetric component of the ST-FMR resonance is by far the dominant contribution, so we will focus on $\vec{\tau}_{\perp}$ here in the main text. The symmetric ST-FMR component indicates only a weak in-plane antidamping torque with Rashba symmetry $\vec{\tau}_{\parallel} \propto \hat{m} \times (\hat{m} \times \hat{y})$ and in some cases a small contribution $\propto \hat{m} \times \hat{z}$ that is not consistent from sample to sample and might arise from strain[23] (see Supporting Information).

Figure 2a shows V_A as a function of ϕ for $TaTe_2$/Py Device 1. The observed $V_A(\phi)$ clearly lacks $\phi \rightarrow -\phi$ symmetry and therefore cannot be described as arising solely from Rashba-like torques $\propto \cos(\phi)$. Other symmetries are allowed, however, in low-symmetry samples such as $TaTe_2$/Py. Torques associated with Dresselhaus-like spin generation (Fig. 1b) can contribute components $\vec{\tau}_{\parallel} \propto \hat{m} \times [\hat{m} \times [\cos(2\phi_{I-ac})\hat{y} \pm \sin(2\phi_{I-ac})\hat{x}]]$ and $\vec{\tau}_{\perp} = \hat{m} \times [\cos(2\phi_{I-ac})\hat{y} \pm \sin(2\phi_{I-ac})\hat{x}]$ where $\hat{x}$ is the direction of applied current. The parts of the Dresselhaus contributions proportional to $\hat{m} \times (\hat{m} \times \hat{x})$ or $\hat{m} \times \hat{x}$ will give torque amplitudes $\propto \sin(2\phi_{I-ac})\sin(\phi)$. We will refer to any current-induced torque of this form as Dresselhaus-like, regardless of its microscopic origin. If we model the out-of-plane torques in

our $TaTe_2$/Py bilayers as a sum of Rashba-like and Dresselhaus-like terms, we can fit V_A as:

$$V_A = \sin(2\phi)\left[A\cos(\phi) + C\sin(\phi)\right], \tag{3}$$

where the $\sin(2\phi)$ dependence comes from the AMR ($dR/d\phi$) in Eq. 2, and both A and C might depend on ϕ_{I-ac}. We extract a value of $C/A = -0.69 \pm 0.01$ for Device 1, in which ϕ_{I-ac} is positive. In Fig. 2b we show $V_A(\phi)$ for $TaTe_2$/Py Device 2, in which ϕ_{I-ac} is negative. Positive and negative values of ϕ_{I-ac} are as defined in Fig. 2c and d respectively. In Device 2 the sign of the $\phi \rightarrow -\phi$ symmetry breaking is opposite that in Device 1, corresponding to an opposite sign $C/A = 0.38 \pm 0.01$. This is consistent with the expectation that in a Dresselhaus-like symmetry the component of spin or field along the current direction changes sign across the mirror plane (Fig. 1b). We note that the observation of a torque $\propto \hat{m} \times \hat{x}$ is distinct from our previously-published work on WTe_2/Py,[10,11] in which we observed a different non-Rashba component of $\vec{\tau}_\perp \propto \hat{m} \times (\hat{m} \times \hat{z})$. A torque proportional to $\hat{m} \times (\hat{m} \times \hat{z})$ for an in-plane magnetization amounts to adding a term constant in ϕ to Eq. 3 (B), such that $\tau_\perp = A\cos(\phi) + B + C\sin(\phi)$. We observe no out-of-plane antidamping torque in our $TaTe_2$/Py devices within experimental uncertainty, even though such a torque is symmetry-allowed in the heterostructure.

We have performed torque measurements on 19 different $TaTe_2$/Py devices (4 2nd-harmonic Hall devices and 15 ST-FMR devices), all with distinct values of ϕ_{I-ac} and $TaTe_2$ thicknesses, t_{TMD}. Figure 3 shows extracted values of C/A as a function of ϕ_{I-ac} for both types of samples. The measurements are in good agreement with the dependence on ϕ_{I-ac} expected for a field or spin polarization with Dresselhaus symmetry (Fig. 1b): C/A goes to zero when the current is applied either along or perpendicular to a mirror plane ($\phi_{I-ac} = 0^o$, 90^o, and 180^o), and changes sign as ϕ_{I-ac} crosses the $TaTe_2$ mirror plane ($\phi_{I-ac} = 0^\circ$). Details for each device are given in the Supporting Information.

To obtain a more quantitative estimate for the strength of the Dresselhaus-like torques,

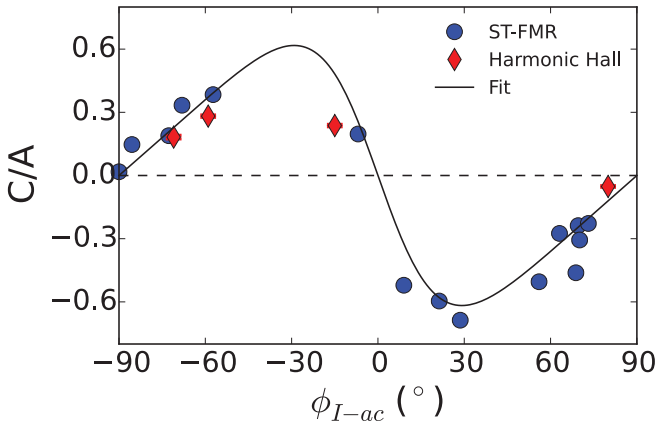

Figure 3: Ratio of torques $\propto \hat{m} \times \hat{x}$ to the torques $\propto \hat{m} \times \hat{y}$, C/A, as a function of the angle between the applied current and the $TaTe_2$ a-c mirror plane for devices studied by either ST-FMR (blue circles) or second harmonic Hall measurements (red diamonds). The fit is discussed in the Supporting Information.

we take into account that a Dresselhaus torque does not point exclusively in the direction $\vec{\tau}_\perp \propto \hat{m} \times \hat{x}$, but depending on the value of ϕ_{I-ac} it can also have a component in the perpendicular direction that can add to or subtract from a component with Rashba symmetry (see Fig. 1a,b):

$$\tau_\perp^C = C\sin(\phi) = [D\sin(2\phi_{I-ac})]\sin(\phi),$$

$$\tau_\perp^A = A\cos(\phi) = [R + D\cos(2\phi_{I-ac})]\cos(\phi),$$

where R is the component of $\cos(\phi)$ torques arising from a Rashba-like symmetry, and D for Dresselhaus-like. The fit lines shown in Fig. 3 for $TaTe_2$/Py corresponds to a value $D/R = -0.51 \pm 0.03$ (see Supporting Information).

We now turn to consideration of the microscopic mechanism that generates current-induced torques with Dresselhaus-like symmetry in our system. $TaTe_2$ cannot generate a torque with a Dresselhaus symmetry through the mechanism present in GaMnAs[12,13] and NiMnSb[16] (a bulk inverse spin Galvanic effect), since inversion symmetry is intact in the $TaTe_2$ bulk. An *interfacial* spin-orbit-torque mechanism is symmetry-allowed, but this would imply a dependence on the $TaTe_2$ thickness that is inconsistent with our measurements (see

Supporting Information). In fact, the measured thickness dependence of the Dresselhaus-like term tracks that of the conventional Rashba-symmetry field-like torque (see Supporting Information), suggesting that both arise from a current-generated Oersted field (see Supporting Information). Furthermore, preliminary first-principles modeling of interfacial spin-orbit torques via a "hidden spin-polarization" mechanism[24–26] (where symmetry mandates that any current-induced spin-polarization on one Te surface must be equal but opposite to the spin-polarization on the opposing Te surface within a single $TaTe_2$ layer) suggests that this effect is small in our system. Finally, except for the conventional Oersted torque and the Dresselhaus-like torque, our measurements indicate that all other components of current-induced torque in $TaTe_2$/Py are small or zero, including the in-plane antidamping torque with Rashba symmetry, $\propto \hat{m} \times (\hat{m} \times \hat{y})$, that is usually dominant in spin-orbit systems. We conclude that direct spin-orbit torques are simply weak in this system (which is likely the reason that $TaTe_2$ does not exhibit an out-of-plane antidamping torque $\propto \hat{m} \times (\hat{m} \times \hat{z})$ even though it is symmetry allowed).

We suggest, instead of a spin-orbit-torque mechanism, that the Dresselhaus-like torque arises from in-plane resistivity anisotropy within the TMD. $TaTe_2$, along with other low symmetry TMDs such as WTe_2 and 1T'-$MoTe_2$, exhibits significant resistance anisotropy. We show the extracted resistivity of $TaTe_2$ from our devices as a function of ϕ_{I-ac} in Fig 4a (where we have removed contributions from the Py layer and contact resistance as outlined in the Supporting Information). The extracted in-plane resistivity anisotropy is 2.6±0.6. When an electric potential is applied away from one of the principal axes in a material with anisotropic resistivity, the electric field and the current are no longer collinear, *i.e.* for a potential along the sample bar the generated current may be tilted. In a bar consisting of just one material, say $TaTe_2$, the boundary conditions force the transverse current at the edges of the bar to be zero. However, in a bilayer with Py, the transverse component of current in the TMD will turn into the Py to establish a return current flowing in the reverse transverse direction and result in a circulating transverse current loop. The Oersted

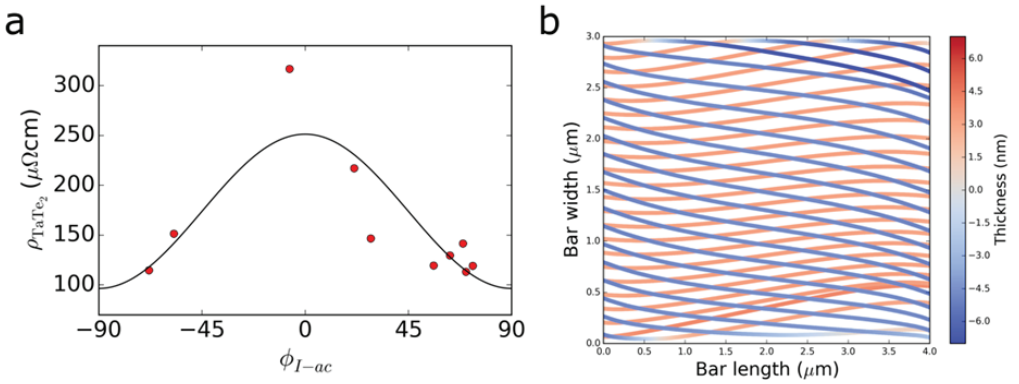

Figure 4: a) Measurement of the $TaTe_2$ resistivity for 10 of our devices as a function of ϕ_{I-ac}, extracted from the two-point resistance. (b) Simulated current paths for a $TaTe_2$(10 nm)/Py(6 nm) bilayer bar of length 4 μm and width 3 μm with $\phi_{I-ac} = 45°$ for a constant voltage applied across the length of the bar. The color map shows the height of the current streamline, with positive values in the Py layer and negative values in the $TaTe_2$ layer.

field generated by this current loop naturally produces a field-like torque on the Py layer that mimics Dresselhaus symmetry ($\vec{\tau}_\perp \propto \sin(2\phi_{I-ac})\hat{m} \times \hat{x}$), in addition to the standard Oersted torque with a Rashba symmetry from the projection of current flowing along the bar. We have modeled the current pathways and associated Oersted fields in our $TaTe_2$/Py bilayers through the finite element analysis software package COMSOL. Figure 4b shows the simulated current path for a constant voltage applied across the length of a $TaTe_2$/Py heterostructure (length 4 μm and width of 3 μm) with an in-plane resistivity anisotropy ratio of 2.6 in the $TaTe_2$. We consider the case that the principle axes of the $TaTe_2$ crystal are tilted at a 45° angle from the length of the bar ($\phi_{I-ac} = 45°$). The blue streamlines show the current within the $TaTe_2$, and the red streamlines show the current flowing within the Py.

By taking the ratio of the integrated total current within the $TaTe_2$ layer going in the y-direction (along the width of the bar) to that in the x-direction (along the length of the bar) we can estimate a value of C/A due to the Oersted field generated by tilted currents. The result has the same dependence on ϕ_{I-ac} as measured for the $TaTe_2$/Py bilayers and the correct overall sign of C/A vs. ϕ_{I-ac} for $TaTe_2$/Py. For an anisotropy ratio of 2.6 we estimate a ratio of $C/A \sim 0.32$, within a factor of 2 of the result found in experiment. The

quantitative difference might be explained by an underestimate of the resistivity anisotropy in the $TaTe_2$ or by spatial non-uniformity in the resistivity of the Py layer as a function of thickness. In the HAADF-STEM imaging (Fig. 1d) we observe some intermixing at the $TaTe_2$/Py interface in a region of approximately one $TaTe_2$ layer thickness. If this disorder causes increased scattering in the Py near the $TaTe_2$/Py interface, the average effective resistivity of the Py would be higher below the midplane of the Py layer than above. This would cause the return current of the transverse current loop flowing in the Py to add to the Oersted field from the transverse current flowing in the $TaTe_2$, while the longitudinal current in the Py at the same time subtracts from the standard Oersted field produced by the longitudinal current in the $TaTe_2$. This has the overall effect of increasing C and decreasing A, giving an enhanced value of C/A.

Previously, our group has studied current-generated torques from another low-symmetry TMD, WTe_2, finding a different unusual component of spin-orbit torque – an out-of-plane antidamping torque – consistent with the WTe_2 crystal symmetries. Like $TaTe_2$, WTe_2 has in-plane resistivitity anisotropy, on the order of 2, so one should expect a field-like torque component with Dresselhaus-like symmetry there as well. In our previous work on WTe_2/Py samples,[10,11] we studied primarily devices with current applied near high symmetry directions ($\phi_{I-bc} = 0^\circ$ and $\pm 90^\circ$) and the Dresselhaus contribution was sufficiently small that we did not make note of it. Nevertheless, measurements of WTe_2/Py devices at intermediate angles ϕ_{I-bc} allow a clear separation of the different torque components based on their dependence on ϕ, and we do indeed observe a Dresselhaus-like component with $D/R = -0.13 \pm 0.02$ (see Supporting Information). The addition of this Dresselhaus-like torque in the analysis of our WTe_2/Py samples does not affect any of our previous conclusions about the strength of the out-of-plane antidamping torque.

In summary, we have measured current-induced torques with Dresselhaus-like symmetry in both $TaTe_2$/Py and WTe_2/Py heterostructures. We explain this torque component not by a direct spin-orbit-torque mechanism, but rather as due to the Oersted field generated

by a component of current transverse to the applied voltage in the sample, arising from the in-plane resistivity anisotropy in the $TaTe_2$. This interesting effect should be present in all spin-orbit-torque heterostructures containing low-symmetry materials with in-plane resistivity anisotropy. It must therefore be taken into account when analyzing the angular dependence of spin-orbit torques in these systems, and when engineering low-symmetry materials to produce spin-orbit torques.

Acknowledgements: The primary support for this project including support for G.M.S., who performed the sample fabrication, electronic and Raman spectroscopy measurements, and data analysis, came from the US Department of Energy (DE-SC0017671). G.M.S. wrote the manuscript with D.C.R. D.M. assisted with device fabrication and data analysis of with support from the National Science Foundation (NSF) (DMR-1708499). N.S. contributed ab-initio modeling and discussion with support from the NSF through the Platform for the Accelerated Realization, Analysis, and Discovery of Interface Materials (PARADIM) (DMR-1539918) and the Cornell University Center for Advanced Computing at Cornell University. I.E.B. performed the electron microscopy under support from the NSF through PARADIM as part of the Materials for Innovation Platform Program. M.H.D.G. contributed to the data analysis and Raman measurements with support from the Kavli Institute at Cornell for Nanoscale Science and the Netherlands Organization for Scientific Research (NWO Rubicon 680-50-1311). N.D.R. contributed experimental assistance with support by the NSF through the Cornell Center for Materials Research (CCMR) (DMR-1719875). L.F.K., C.F., R.A.B., and D.C.R. supervised the research. All authors contributed to the final version of the manuscript. Sample fabrication was performed in the CCMR shared facilities and at the Cornell Nanoscale Science & Technology Facility, part of the National Nanotechnology Coordinated Infrastructure, which is supported by the NSF (ECCS-1542081). The FEI Titan Themis 300 was acquired through Grant NSF-MRI-1429155, with additional support from Cornell University, the Weill Institute, and the Kavli Institute at Cornell.

References

1. Brataas, A.; Kent, A. D.; Ohno, H. Current-induced torques in magnetic materials. Nature Materials **2012**, 11, 372.

2. Liu, L.; Moriyama, T.; Ralph, D. C.; Buhrman, R. A. Spin-Torque Ferromagnetic Resonance Induced by the Spin Hall Effect. Physical Review Letters **2011**, 106, 036601.

3. Liu, L.; Pai, C.-F.; Li, Y.; Tseng, H. W.; Ralph, D. C.; Buhrman, R. A. Spin-Torque Switching with the Giant Spin Hall Effect of Tantalum. Science **2012**, 336, 555–558.

4. Miron, I. M.; Gaudin, G.; Auffret, S.; Rodmacq, B.; Schuhl, A.; Pizzini, S.; Vogel, J.; Gambardella, P. Current-driven spin torque induced by the Rashba effect in a ferromagnetic metal layer. Nature materials **2010**, 9, 230–4.

5. Sánchez, J. C. R.; Vila, L.; Desfonds, G.; Gambarelli, S.; Attané, J. P.; De Teresa, J. M.; Magén, C.; Fert, A. Spin-to-charge conversion using Rashba coupling at the interface between non-magnetic materials. Nature Communications **2013**, 4, 2944.

6. Mellnik, A. R.; Lee, J. S.; Richardella, A.; Grab, J. L.; Mintun, P. J.; Fischer, M. H.; Vaezi, A.; Manchon, A.; Kim, E.-A.; Samarth, N. et al. Spin-transfer torque generated by a topological insulator. Nature **2014**, 511, 449.

7. Fan, Y.; Upadhyaya, P.; Kou, X.; Lang, M.; Takei, S.; Wang, Z.; Tang, J.; He, L.; Chang, L.-T.; Montazeri, M. et al. Magnetization switching through giant spin-orbit torque in a magnetically doped topological insulator heterostructure. Nature Materials **2014**, 13, 699–704.

8. Amin, V. P.; Stiles, M. D. Spin transport at interfaces with spin-orbit coupling: Formalism. Physical Review B **2016**, 94, 104419.

9. Amin, V. P.; Stiles, M. D. Spin transport at interfaces with spin-orbit coupling: Phenomenology. Physical Review B **2016**, 94, 104420.

10. MacNeill, D.; Stiehl, G. M.; Guimaraes, M. H. D.; Buhrman, R. A.; Park, J.; Ralph, D. C. Control of spin-orbit torques through crystal symmetry in WTe_2/ferromagnet bilayers. Nature Physics **2017**, 13, 300–305.

11. MacNeill, D.; Stiehl, G. M.; Guimarães, M. H. D.; Reynolds, N. D.; Buhrman, R. A.; Ralph, D. C. Thickness dependence of spin-orbit torques generated by WTe_2. Physical Review B **2017**, 96, 054450.

12. Fang, D.; Kurebayashi, H.; Wunderlich, J.; Výborný, K.; Zârbo, L. P.; Campion, R. P.; Casiraghi, A.; Gallagher, B. L.; Jungwirth, T.; Ferguson, A. J. Spin-orbit-driven ferromagnetic resonance. Nature Nanotechnology **2011**, 6, 413–417.

13. Kurebayashi, H.; Sinova, J.; Fang, D.; Irvine, A. C.; Skinner, T. D.; Wunderlich, J.; Novák, V.; Campion, R. P.; Gallagher, B. L.; Vehstedt, E. K. et al. An antidamping spin-orbit torque originating from the Berry curvature. Nature Nanotechnology **2014**, 9, 211–217.

14. Skinner, T. D.; Olejník, K.; Cunningham, L. K.; Kurebayashi, H.; Campion, R. P.; Gallagher, B. L.; Jungwirth, T.; Ferguson, A. J. Complementary spin-Hall and inverse spin-galvanic effect torques in a ferromagnet/semiconductor bilayer. Nature Communications **2015**, 6, 6730.

15. Chen, L.; Decker, M.; Kronseder, M.; Islinger, R.; Gmitra, M.; Schuh, D.; Bougeard, D.; Fabian, J.; Weiss, D.; Back, C. H. Robust spin-orbit torque and spin-galvanic effect at the Fe/GaAs (001) interface at room temperature. Nature Communications **2016**, 7, 13802.

16. Ciccarelli, C.; Anderson, L.; Tshitoyan, V.; Ferguson, A. J.; Gerhard, F.; Gould, C.; Molenkamp, L. W.; Gayles, J.; Železný, J.; Šmejkal, L. et al. Room-temperature spin-orbit torque in NiMnSb. Nature Physics **2016**, 12, 855–860.

17. Aradhya, S. V.; Rowlands, G. E.; Oh, J.; Ralph, D. C.; Buhrman, R. A. Nanosecond-Timescale Low Energy Switching of In-Plane Magnetic Tunnel Junctions through Dynamic Oersted-Field-Assisted Spin Hall Effect. Nano Letters **2016**, 16, 5987–5992.

18. Brown, B. E. The crystal structures of $NbTe_2$ and $TaTe_2$. Acta Crystallographica **1966**, 20, 264–267.

19. Srgel, T.; Nuss, J.; Wedig, U.; Kremer, R.; Jansen, M. A new low temperature modification of $TaTe_2$ — Comparison to the room temperature and the hypothetical 1T-$TaTe_2$ modification. Materials Research Bulletin **2006**, 41, 987 – 1000.

20. Li, J.; Haney, P. M. Interfacial magnetic anisotropy from a 3-dimensional Rashba substrate. Applied Physics Letters **2016**, 109, 032405.

21. Hayashi, M.; Kim, J.; Yamanouchi, M.; Ohno, H. Quantitative characterization of the spin-orbit torque using harmonic Hall voltage measurements. Phys. Rev. B **2014**, 89, 144425.

22. Avci, C. O.; Garello, K.; Gabureac, M.; Ghosh, A.; Fuhrer, A.; Alvarado, S. F.; Gambardella, P. Interplay of spin-orbit torque and thermoelectric effects in ferromagnet/normal-metal bilayers. Phys. Rev. B **2014**, 90, 224427.

23. Guimarães, M. H. D.; Stiehl, G. M.; MacNeill, D.; Reynolds, N. D.; Ralph, D. C. Spin-Orbit Torques in $NbSe_2$/Permalloy Bilayers. Nano Letters **2018**, 18, 1311–1316.

24. Zhang, X.; Liu, Q.; Luo, J.-W.; Freeman, A. J.; Zunger, A. Hidden spin polarization in inversion-symmetric bulk crystals. Nature Physics **2014**, 10, 387–393.

25. Železný, J.; Gao, H.; Manchon, A.; Freimuth, F.; Mokrousov, Y.; Zemen, J.; Mašek, J.; Sinova, J.; Jungwirth, T. Spin-orbit torques in locally and globally noncentrosymmetric crystals: Antiferromagnets and ferromagnets. Physical Review B **2017**, 95, 014403.

26. Wadley, P.; Howells, B.; Železný, J.; Andrews, C.; Hills, V.; Campion, R. P.; Novák, V.; Olejník, K.; Maccherozzi, F.; Dhesi, S. S. et al. Electrical switching of an antiferromagnet. Science **2016**, 351, 587–590.